Available online at www.sciencedirect.com

SciVerse ScienceDirect

Ceramics International 38 (2012) 5907–5914

CERAMICS INTERNATIONAL

www.elsevier.com/locate/ceramint

Synthesis, sintering and ionic conductivity of scandia-doped ceria ceramic materials obtained by different procedures

A. Moure [a,*], A. Castro [b], I. Martinez [b], C. Moure [a], J. Tartaj [a]

[a] Instituto de Cerámica y Vidrio, CSIC, C/Kelsen, 5, 28049 Madrid, Spain

[b] Instituto de Ciencia de Materiales de Madrid, CSIC, c/Sor Juana Inés de la Cruz, 3, Cantoblanco, 28049 Madrid, Spain

Received 12 March 2012; received in revised form 13 April 2012; accepted 13 April 2012

Available online 20 April 2012

Abstract

Crystalline scandia-doped ceria powders, with $Ce_{0.92}Sc_{0.08}O_{2-\delta}$ and $Ce_{0.82}Sc_{0.18}O_{2-\delta}$ compositions have been prepared by three different procedures: (a) mechanochemical route from the starting oxides; (b) co-precipitation of hydroxides from an aqueous solution; (c) solid state reaction between oxides. Nanopowders were only obtained from the two first routes. Isothermal sintering was carried out between 1200 and 1500 °C. Apparent density as high as 99% D_{th} was achieved by sintering at 1300 °C for 2 h from co-precipitated powders. Temperature was further reduced, and 99% D_{th} was also obtained by SPS at 950 °C of $Ce_{0.82}Sc_{0.18}O_{2-\delta}$ mechanically activated powders. Sc_2O_3 was observed as a secondary phase for all the samples containing 18 at% Sc, whereas only traces were pointed out in the 8 at% Sc samples. Total conductivity attains lower values than those measured in other ceria solid solutions, at difference of that observed in cubic Sc-stabilized zirconia.

Keywords: Milling; Fuel cells; CeO_2; Ionic conductivity; Spark plasma sintering

1. Introduction

Rare earth doped ceria is a well known candidate for uses as electrolyte material for low temperature (500–700 °C) solid oxide fuel cell (LT-SOFC) applications due to their oxygen ion conductivity, which is higher than that of the yttria-stabilized zirconia [1–5] at lower temperatures. Although the conductivity of RE-doped ceria is, in average, higher than that corresponding to RE-doped zirconia, differences of conductivity exist due to the RE cation nature. Thus, Sm-doped ceria has proved to have higher conductivity than Y-doped ceria [6,7]. According to M. Yashima et al. [6] there is not a monotone correlation between the ionic radius of the RE cation and the ionic conductivity (σ). Thus, Y-doped ceria shows better values of σ than the Nd- and La-doped ceria. Improvement of ionic conductivity has also been attained by co-doping with two RE cations [8]. On the other hand, Sc-doped ZrO_2 has proved to be the best ionic conductor in the group of RE_2O_3-doped ZrO_2 solid electrolytes for uses in SOFC technology [9]. Use of scandium oxide as an additive to CeO_2 to modify the ionic conductivity is scarcely documented. Solid solutions with relatively high scandium oxide content have shown that the solid solution limit is low [10], and two-phase materials are formed above 8–10 at% Sc_2O_3. The main reason for this behaviour is associated to the strong difference between the ionic radii of both host lattice cation Ce^{4+} and Sc^{3+}, 0.97 Å and 0.87 Å in 8-fold co-ordination, respectively. In the present work, the structural, microstructural and ionic conduction behaviour of 8 at% and 18 at% of Sc-doped CeO_2 limit compositions are studied. The 18 at% composition was chosen to make a comparison with similar $Ce_{0.82}RE_{0.18}O_{2-\delta}$ compositions [11], while the 8 at% was chosen because this amount seems to be the upper limit reported to incorporate Sc to fluorite CeO_2 forming a solid solution [10]. To overcome the difficulty to prepare the Sc-CeO_2 solid solution, mechanochemical and chemical co-precipitation synthesis routes were used to obtain good quality powders, such as have been proved in other systems [12]. Solid-state reaction was used as the reference procedure. These routes were employed with the aim of increasing the solubility of Sc in ceria, and to study the influence in the possible improvement of the properties with compositions not previously reported.

* Corresponding author.
E-mail address: alberto.moure@icv.csic.es (A. Moure).

0272-8842/$36.00
http://dx.doi.org/10.1016/j.ceramint.2012.04.041

2. Experimental methods

Ceria powders containing 18 or 8 mol% Sc cations were prepared by different ways: co-precipitation of hydroxides from an aqueous solution of the Ce and Sc nitrates, $(Ce(NO_3)_3)\cdot 6H_2O$ (99.5%, Alfa Aesar) and $Sc(NO_3)_2\cdot 4H_2O$ (99.0%, Alfa Aesar) (18Chem hereafter) and mechanical activation from oxides mixture (18MEC hereafter) for 18 mol% $ScO_{1.5}$. The 8 mol% composition was prepared by conventional solid state reaction of a mixture of oxides (8SSR hereafter) and mechanical activation from the same mixture of oxides (8MEC hereafter). The 18Chem powder was obtained by a previously described route [11]. 18MEC and 8MEC powders were obtained after 24 h of high-energy milling. The stoichiometric quantities of CeO_2 and Sc_2O_3, necessary to obtain 10 g of the ceramic precursors were placed in a Tungsten carbide (WC) pot with seven also WC balls, 2 cm diameter, 35 g each. The mechanical treatment was carried out in a Pulverisette 6 model Fritsch planetary mill operating at 300 rpm. More details for this way on CeO_2-based solid solutions are given by A. Moure et al. [13]. The solid solution formation was studied by powder X-ray diffraction (XRD) analysis. The 8SSR powder was obtained by calcinations at 1000 °C during 2 h of a stoichiometric mixture of both oxides, after homogenization by attrition milling.

For the co-precipitation method, TG/ATD analysis was only performed on the dried precipitate. The calcined powder was attrition milled with isopropanol as liquid medium. All the powders were controlled by XRD diffraction, with a Bruker AXS D8 Advance diffractometer, Madison, WI. Crystallite size was determined by line-broadening analysis of the XRD patterns. For MEC powder, the modification of the particle size as a function of the milling time was calculated by XRD using the Debye–Scherrer formulae

$$d_{\mathrm{XRD}} = \frac{0.9\lambda}{\beta \cos\theta}, \tag{1}$$

$$\beta^2 = \beta^2_{\mathrm{sample}} - \beta^2_{\mathrm{inst}}, \tag{2}$$

where β_{inst} corresponds to the equipment broadening, taken from well-crystallized Si pattern and β_{sample} is the broadening of the corresponding diffraction peaks at 2θ. BET characterization was carried out with by using a Quantachrome MS-16 model, Syosset, NY.

18Chem, 8MEC and 8SSR powders were isostatically pressed at 150 MPa. 18MEC powder was densified by Spark Plasma Sintering, in a SPS 2080 Sumitomo apparatus, (Osaka, Japan) at 950 °C for 1 min, and 120 MPa. Constant heating rate (CHR) essays were performed on a Dilatometer (Netzsch 402E of Geratebau, Bayern, Germany), from room temperature up to 1600 °C at a constant heating rate of 5 °C/min. Isothermal sintering of 18Chem, 8MEC and 8SSR powders was conducted at several temperatures between 1200 °C and 1500 °C and times ranging from 1 to 16 h, with heating and cooling rates of 3 °C/min. Apparent density was measured by Archimedes method. XRD analysis was carried out to determine the complete solid solution formation and the crystallization of the ceramic bodies. Lattice parameters of the solid solution members (0.5413 ± 0.0001 nm and 0.5408 ± 0.0001 nm for $Ce_{0.92}Sc_{0.08}O_{2-\delta}$ and $Ce_{0.82}Sc_{0.18}O_{2-\delta}$, respectively) were determined from the XRD data obtained with a scanning of 1/8 2θ/min between 20° and 60° 2θ, and using Si as internal standard. Microstructure was observed by scanning electron microscope of polished and thermally etched surfaces, in a FE-SEM, model Hitachi S-4700, Tokyo, Japan.

Complex impedance spectroscopy (CIS) was employed to determine the bulk, grain boundary (G.B.) and total ionic conductivity at a temperature range between 200 °C and 600 °C, and 100–10^8 Hz frequency range, by using a HP 4294A impedance meter (Agilent, Palo Alto, CA). Ag paste was applied on the surface of sintered discs. Electrodes were fired at 750 °C 1 h. Surface resistance values lower than 0.1 Ω were attained on the fired electrodes. Bauerle model of equivalent RC parallel circuits has been taken to separate bulk and G.B. contributions [14]. Conductivity values from the spectroscopic diagrams have been calculated by impedance data taken on the bulk and G.B. arcs by the formula $\sigma = (1/Z')x(l/S)$, being l and S thickness and surface, respectively, measured on the disc samples. The value $\sigma = (1/Z'_{\mathrm{GB}}) \times (l/S)$ has been taken as an average G.B. value for the sake of comparison between different samples and as representative of the electrical G.B. behaviour of the ceramic electrolyte.

3. Results and discussion

Fig. 1 shows the results obtained by DTA/TG analysis of the precipitated 18Chem powder after washing. It shows that the weight loss ends at 600 °C, although this end is practically achieved at 500 °C. This is the temperature chosen for the calcinations of the precipitate. Fig. 2 shows the XRD pattern of this powder heated at 500 °C for 2 h. The pattern apparently corresponds to a fluorite structure ($Ce_{1-x}Sc_xO_{2-\delta}$), in which traces of Sc_2O_3 can be also appreciated. This secondary phase seems to disappear when the sintering temperature of the 18Chem precursors increases, as it is shown in Fig. 2, at least at the limit of the XRD technique.

Fig. 3a displays the XRD patterns of the 18MEC mixture evolution as a function of the milling time. In the initial

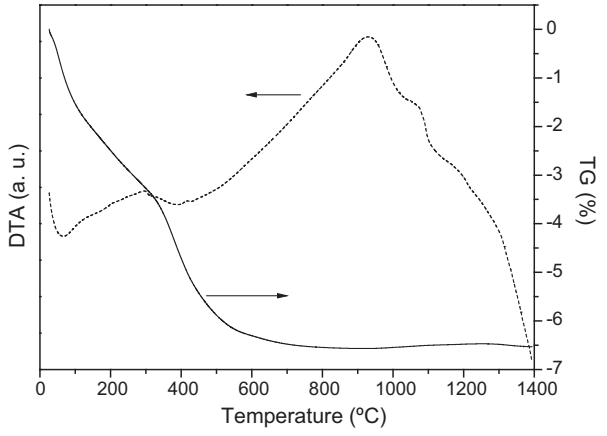

Fig. 1. DTA-TG curves of 18Chem dried powders.

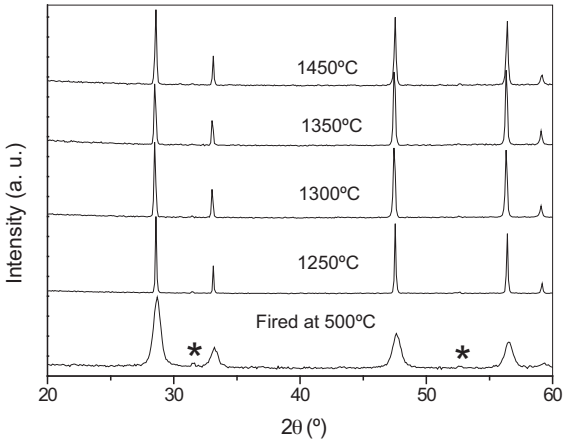

Fig. 2. XRD pattern of 18Chem sample fired at 500 °C and ceramics sintered from that powder at different temperatures (*peaks corresponding to Sc_2O_3).

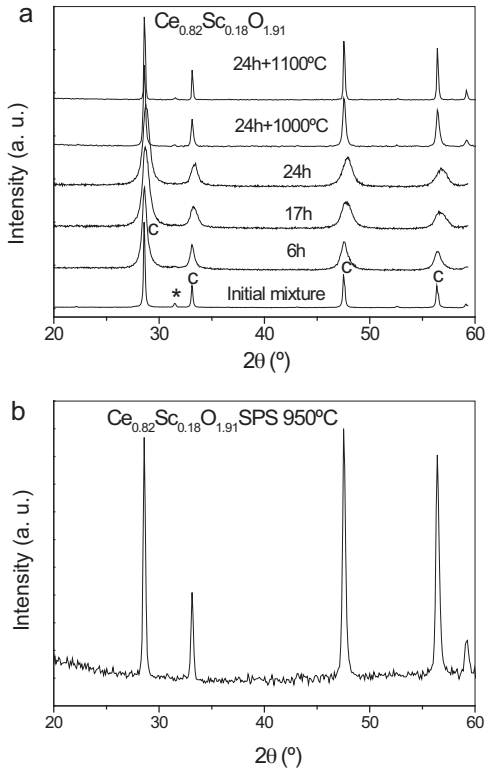

Fig. 3. XRD patterns of 18MEC sample: (a) the evolution of powder with milling time (6, 17, 24 h) and the evolution of milled powder against temperature; (b) XRD patterns of the ceramics processed by SPS at 950 °C from the milled 18MEC powder (c: peaks corresponding to CeO_2; *Sc_2O_3).

mixture, the peaks corresponding to the CeO_2 and Sc_2O_3 are shown. When the milling time increases the peaks corresponding to Sc_2O_3 disappear from the patterns. This mechanical treatment seems to favour the formation of the solid solution with relatively high amounts of Sc_2O_3 incorporated to the structure. Fig. 3a also shows the XRD patterns of the powder mechanosynthesized during 24 h after thermal treatments at 1000 and 1100 °C. A compacted disc was treated at different temperatures, for 1 h at each temperature, thus the same sample was used for all the treatments. At 1100 °C it can be observed that traces of Sc_2O_3 seem to be ex-solved from the former solid solution. To assure the processing of a dense and crystalline ceramic with the highest amount of Sc incorporated to the structure, SPS of 18MEC precursors at 950 °C was tested. Fig. 3b shows the XRD pattern of the sample prepared by such method. It seems that the solid solution is complete and peaks corresponding to Sc_2O_3 are difficult to be observed, within the limits of the technique. That is, secondary Sc_2O_3 oxide could be present in the ceramic in small quantities or even in a nearly amorphous state.

Fig. 4 shows the evolution with milling time of the $Ce_{0.92}Sc_{0.08}O_{1.96}$ composition prepared by mechanochemical route (8MEC). The powder obtained after 24 h of milling process shows a nanometric size. The crystallite size decreases as milling time increases, according to that measured by XRD broadening, from 91 nm for the initial mixture to 13 nm, approximately, after milling during 24 h. The XRD patterns corresponding to the ceramics sintered at different temperatures from the 8MEC powders milled during 24 h are shown in Fig. 4. The peaks corresponding to Sc_2O_3 are more difficult to be distinguished in the whole range of sintering temperature, mainly at temperatures higher than 1200 °C. It reflects that ceramics with 8 at% Sc can be obtained by a single thermal step from mechanosynthesized precursors.

Fig. 5a and b shows the shrinkage and shrinkage rate behaviour, respectively, of the powders obtained by the different methods. The processes at low temperatures correspond to the release of some organic rests in the case of the 18Chem sample. In the case of the milled materials, they can be attributed to the loss of H_2O and CO_2 trapped from the atmosphere in the mixture during milling, as it has been observed in other mechanosynthesized powders [15]. Only the 18Chem powder attains a state of final shrinkage below 1500 °C, while the other samples do not finish their shrinkage at that temperature. The 18MEC powders show two maxima in the shrinkage rate curves at 1280 and 1360 °C, close to the highest temperature corresponding to 18Chem powder (at 1220 °C).

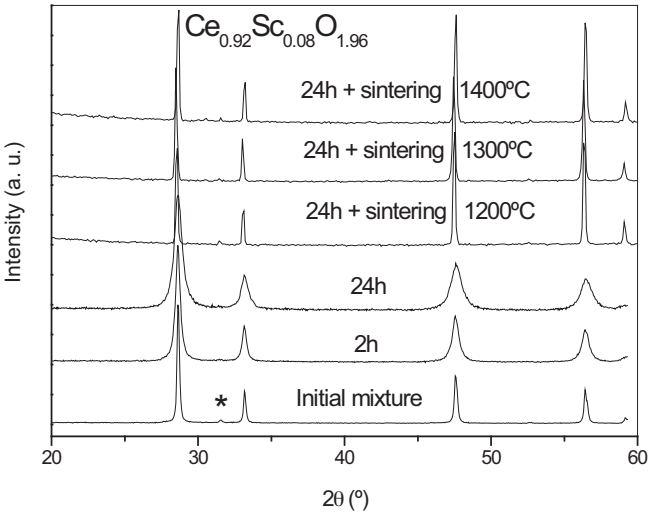

Fig. 4. XRD patterns of 8MEC sample, showing evolution of milling powder with time and those corresponding to the ceramics sintered from the powder obtained by milling during 24 h (*peaks corresponding to Sc_2O_3).

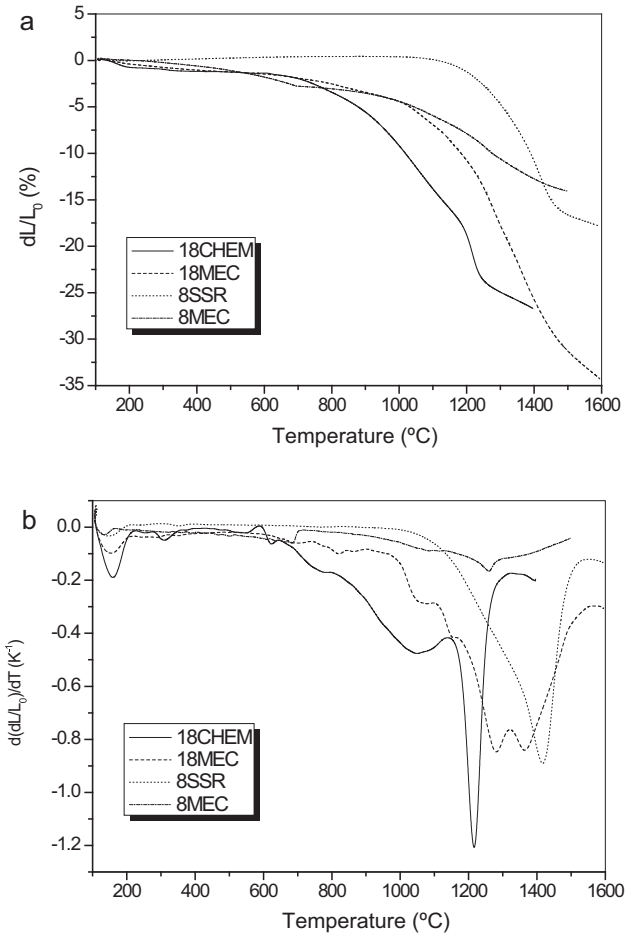

Fig. 5. (a) Shrinkage curves; (b) shrinkage rate curves of green pellets of the ceramic powders processed by the different routes and compositions.

The 8SSR powder shows a maximum at higher temperature (1400 °C), although, on the contrary to the other powders, the shrinkage rate curve is enough homogeneous, with a unique maximum peak. It indicates a more homogeneous pore distribution (not represented here) than the rest of ceramic precursors. According to the results obtained by CHR essays, isothermal sintering has been carried out at different conditions. Table 1 summarizes the values of the relative density as a function of the sintering temperature for each type of sample

Table 1
Apparent density of different samples as a function of sintering temperature (time 2 h, 1 min for SPS).

Temperature (°C)	% D_{th}			
	Sample 18MEC	Sample 18Chem	Sample 8MEC	Sample 8SSR
950 SPS	99.0	–	–	–
1250	–	99.1	–	–
1300	–	99.5	96.0	–
1350	–	99.2	99.0	–
1400	–	98.0	99.7	95.7
1450	–	97.4	99.0	98.9
1500	–	99.0	98.8	96.1
1550	–	–	–	95.8

precursor. Theoretical densities have been calculated from the structural data obtained by XRD of the solid solution, being 6.42 and 6.97 g cm^{-3} for 18 and 8 at% Sc, respectively. However, it must be pointed out that the measured value can be affected by the presence of small quantities of free Sc_2O_3 secondary phase.

Fig. 6 shows the microstructure of the samples corresponding to ceramics processed from the different synthesized powders. The samples sintered from 18Chem powders show a sub-micrometric grain size (Fig. 6a), in which small inclusions of pure Sc_2O_3 are dispersed indicating that the whole amount of Sc has not entirely incorporated in the ceria structure, or it has been ex-solved during sintering at high temperature. The MEC powders led to quite dense ceramics (Fig. 6b) with a nanometric grain size when they are prepared by SPS at 950 °C. Grains of pure Sc_2O_3 are not easily distinguished in these microstructures. If they are present, it may be possible that their small size makes more difficult its microscopic visualization.

Micrographs of 8MEC ceramics sintered at 1400 °C (Fig. 6c) show a microstructure according to the nano-particle nature of the powder. Hence, densification is high, as it is observed in the corresponding microstructure, and secondary phases of pure scandia are not appreciated, in good correspondence with the XRD results. The 8SSR powder led to a microstructure with larger grains (Fig. 6d), and a bimodal distribution. This different behaviour is associated to the high temperatures at which the sintering has been carried out and the larger initial particle size after calcinations at 1000 °C, in the order of 0.7 μm as it is calculated from the specific surface measured by BET method. The average grain size is in the micrometric range and at 1450 °C a bimodal distribution of the grain size is more visible. This is associated with the presence of a secondary phase that can be distinguished by EDS, which corresponds to a small amount of free Sc_2O_3 (not detected by XRD) at difference of that observed in the image of 18MEC. Microstructures are, as expected, in good agreement with the high values of apparent density measured in the sintered samples shown in Table 1.

Fig. 7 shows the impedance arcs corresponding to ceramics sintered from the different powders. They are represented at the temperatures where both bulk and grain boundary arcs are best defined. The Arrhenius plots of the bulk, grain boundary and total conductivity, obtained from the corresponding arcs at different temperatures, are shown in Fig. 8.

The electrical behaviour strongly differs from one another composition. With regard to the ones containing an excess of Sc_2O_3, i.e. 18Chem and 18MEC samples, ionic conductivity is much lower than that with 8 at% (Fig. 8). As it is shown in Fig. 8, the bulk, G.B. and total conductivity of 18 at% compositions are quite lower than those of 8 at% compositions.

The 18MEC sample processed by SPS shows a very fine-grained microstructure, as shown in Fig. 6b. Only bulk arcs have been distinguished on these samples (Fig. 7b), because the G.B. arcs are not well developed at the range of measurement temperature due to the high grain boundary resistivity, and therefore total conductivity at this processing condition cannot be established. This is the reason why it is not represented in

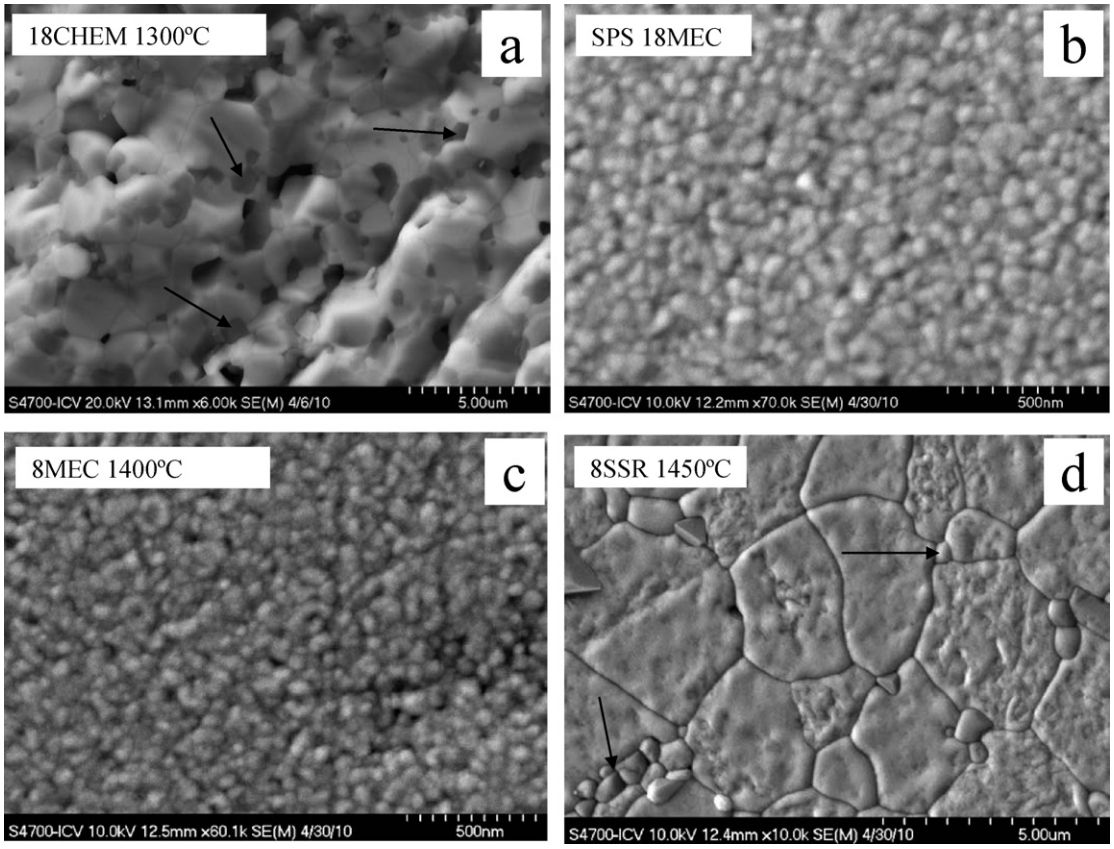

Fig. 6. SEM micrographs of samples corresponding to ceramics processed at: (a) 18CHEM, 1300 °C (fracture); (b) SPS 18MEC, 950 °C; (c) 8MEC, 1400 °C; (d) 8SSR 1450 °C.

Fig. 8. The electrical parameter corresponding to the bulk conductivity is practically one order of magnitude lower than that of the 18Chem ceramic (Fig. 8), although the activation energy is also lower. Both conductivities are rather lower than the corresponding to the same composition in the Sc-ZrO_2 system with 18 at% Sc [16].

As it can be seen, the 8SSR samples with higher grain sizes show a better G.B. conductivity (Fig. 8), and lower activation energy (1.16 eV) than the 18Chem ones (1.46 eV) and similar to 8MEC samples (1.19 eV) at the same sintering temperatures. In these ceramics, well-defined arcs from the different contributions to the resistivity are visible (Fig. 7). Bulk and G.B. conductivities are comparable between them, and the total conductivity is controlled by both mechanisms.

4. Discussion

The results shown in Fig. 2 prove that coprecipitation route is a good method to increase the amount of Sc that can be introduced in the ceria fluorite structure, with respect to the classical method [10]. The high degree of homogenization occurring during the coprecipitation of the oxides together with the relatively high sintering temperatures used seems to be the key factors for this behaviour.

In the same way, mechanosynthesis is also proved to be a useful technique to prepare nano-powders of scandia-modified ceria, in which the solid solution limits can have high values such as 18 at% Sc, well above to that found and reported in the literature. The high homogenization degree and the high mechanical energy introduced by the prolonged milling [12] help the small Sc cations to be accommodated within the ceria structure. Nevertheless, these powders are unstable against thermal treatments above 1000 °C, giving as final phases Sc-modified ceria, with lower Sc amount than the nominal one, and free cubic Sc_2O_3, similarly to what was shown by Grover et al. [10]. To process ceramics with high density maintaining that high content of Sc_2O_3 in solid solution with ceria, SPS technique, i.e. sintering at high pressures and low times process, has to be used. SPS technique allows the small volume of the lattice associated to the small ionic radius of Sc^{3+} to be maintained, without any decomposition of the solid solution.

The conductivity values corresponding to the 8MEC samples are the highest of all the samples measured here. They are 2–3 magnitude order lower than that of the Gd-doped ceria with the same doping extent [17] and also slightly lower than Sc-doped ZrO_2 solid solutions [9,18]. Two contributions to the conductivity, one coming for the changes in the structure by Sc-doping and another coming from the differences observed in the microstructure of the ceramics, explain this behaviour.

The dependence of the conductivity with the incorporation of Sc in the structure must be studied by analysing the behaviour of the bulk conductivity, which is not affected by microstructural features. It differs less than one order of magnitude between both 8 at%-doped samples, and is much

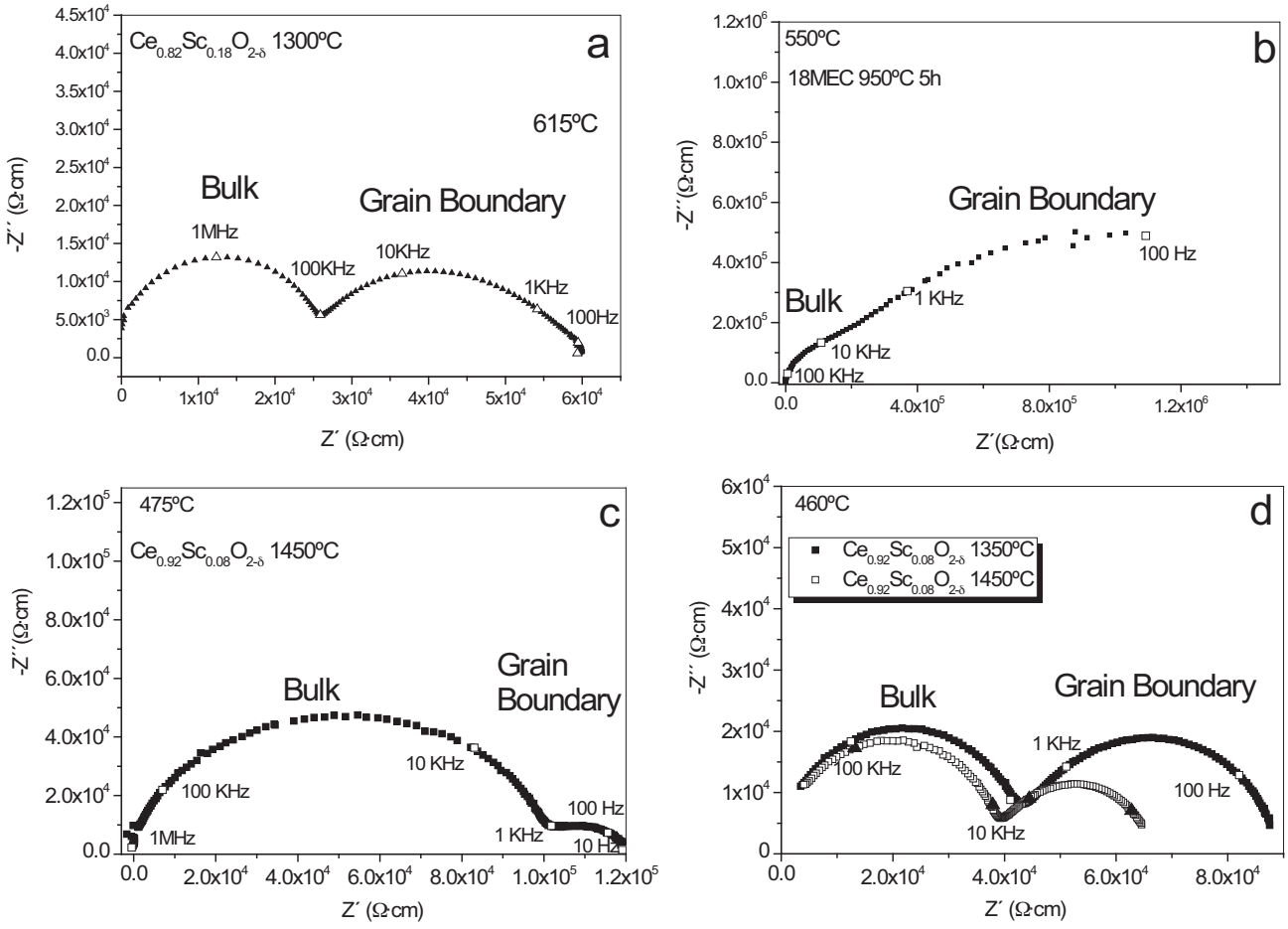

Fig. 7. Impedance arcs measured at different temperatures of: (a) 18CHEM ceramics; (b) SPS 18MEC; (c) 8SSR ceramic treated at 1450 °C; (d) 8MEC ceramic treated at different temperatures.

lower for the 18 at%-doped samples. According to Yashima and Takizawa [6] the conductivity of doped fluorite-type crystalline compound, ZrO_2 and CeO_2 reaches its maximum when the ionic radius value of doping cation is close to the host lattice forming one. Taking into account the difference between the ionic radius of Sc^{3+} and Ce^{4+} ($r_i^{VIII} = 0.87$ and $r_i^{VIII} = 0.97$ Å, respectively), the Sc cation is rather smaller than Ce one. The low solid-solution limit and the decrease of the conductivity value with regard to the other ceria solid solutions, such as Sm-doped and Gd-doped CeO_2, can be attributed to this mismatch between ionic radii of doping and host cations. Some authors have reported [19] that there are more contributions that produce the differences in conductivity beside the strain caused by the difference of ionic radii. However, being Sc^{3+} much smaller than Ce^{4+}, the huge decrease of conductivity can be only attributed to the crystalline structure deformation. The lower bulk conductivity of the 18 at%-doped ceramics can be also influenced by the presence in these samples of a non-conductive Sc_2O_3 phase and a higher resistivity. Taking into account that the conductivity parameter, σ, has been calculated from the formula $\sigma = S \times l/A$ in which l and A are measured on the overall sample, the inclusion of non-conductive phases in a fixed geometry must lead to a decrease of σ because there are lower amounts of a more conductive phases. Slight differences in the bulk conductivity of 8MEC and 8SSR sample, shown in Fig. 8 can be attributed to a slightly different amount of Sc incorporated to the structure. The arcs corresponding to bulk conduction seem to be slightly depressed for 8MEC and 8SSR ceramics. It suggests that some secondary phases could be contributing to the conductivity of both ceramics in a frequency range similar to that one of bulk CeO_2.

Values of conductivity measured on these Sc-doped ceria samples are lower than the corresponding to other solid solutions in which a small RE cation has also been employed, like Y ($r_i^{VIII} = 1.019$ Å), or Yb ($r_i^{VIII} = 0.985$ Å) [11,20]. The size of the lattice cell measured for 8 mol% Sc^{3+} substitutions in ceria is very small, so the oxygen mobility decreases to values close to those corresponding to the RE-doped zirconia, which show conductivity values in the range of the ones measured in this work at similar temperatures. The ionic conductivity has been correlated with the atomic displacement parameters [6]. Thus, lower atomic displacement leads to higher ionic conductivity. In the same way, higher RE ionic radii allow the conductivity to be increased [21]. Due to its very small ionic radius, the Sc^{3+} cation should lead to an atomic displacement higher than the Yb^{3+} cation. Beside, the amount of oxygen vacancies is also an important factor to determine the conductivity parameter. The limit established for solid solution

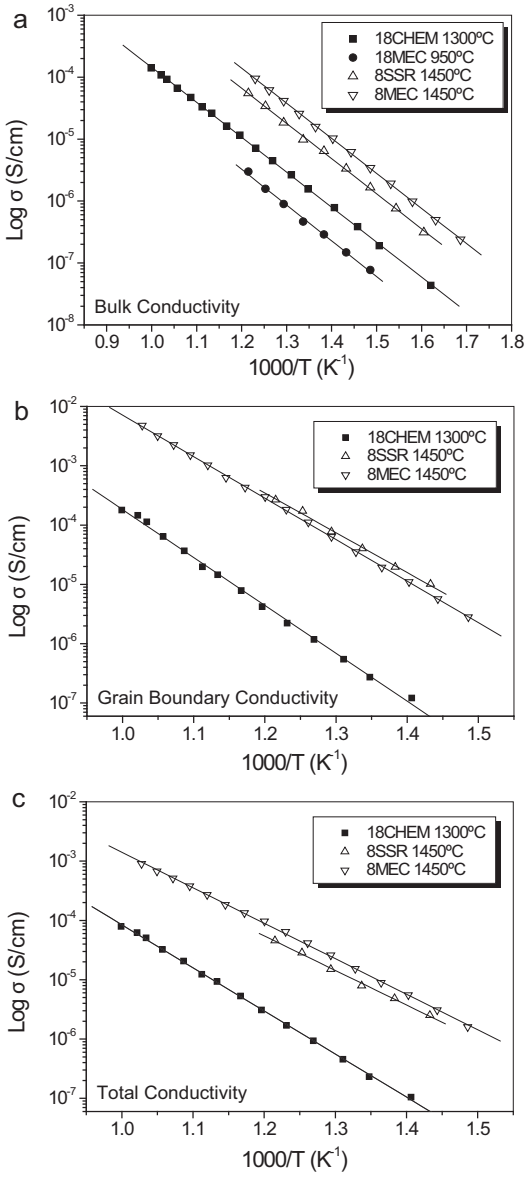

Fig. 8. Arrhenius plots of the (a) bulk, (b) grain boundary and (c) total conductivity of ceramics sintered from the different routes and compositions.

formation with Sc doping makes difficult attaining the high conductivity values measured on other $Ce_{0.80}RE_{0.20}O_{2-\delta}$ solid solutions.

As it is shown in Fig. 8, the values of the total conductivity of 8SSR and 8MEC ceramics are limited by the reduction of the G.B. conductivity with respect to the bulk one. Fig. 7 shows that the arcs corresponding to the grain boundary contribution seem to be depressed. Although it is not detectable by XRD, it is possible that small amounts of secondary phases are segregated to the grain boundary, making the G.B. conductivity to be lower. This fact has also been observed in other SOFC electrolytes candidate materials [11]. Slight differences in the composition and/or distribution of these phases should lead to changes in the conduction behaviour of the corresponding ceramics. The conductivity values here obtained limit the use of these solid solution materials as electrolytes for SOFC to high temperatures.

5. Conclusions

The use of coprecipitation and mechanochemical method has allowed to obtain the doped ceria solid solution metastable powders with percentages as high as 18 at% Sc, which are impossible to attain by standard methods such as solid state reaction and other soft chemical routes. Applying SPS technique to the Sc-rich powder allows dense ceramic bodies to be obtained, in which solid solution seems to be maintained, although the grain boundary and thus the total resistivity of this sample are quite high. Ionic conductivity is lower than that of other ceria doped electrolytes, being closer to the doped zirconia. Ionic conductivity increases when Sc amount decreases. A lower constrain of the lattice cell favoured by low Sc contents could explain this ionic conductivity behaviour. Single phase ceramics with higher final grain sizes show better values for ionic conductivity.

Acknowledgements

This work was supported by Spain MICINN MAT2008-06785-C02-02-E Project. AC and IM acknowledge the financial support of the Spanish MICINN (FR2009-0093 and MAT2011-23709). The authors also thank the assistance of the PFN2, Toulouse, France, where the SPS experiments were performed.

References

[1] V. Esposito, E. Traversa, Design of electroceramics for solid oxides fuel cell applications: playing with ceria, Journal of the American Ceramic Society 91 (4) (2008) 1037–1051.
[2] B.C.H. Steele, Appraisal of $Ce_{1-y}Gd_yO_{2-y/2}$ electrolytes for IT-SOFC operation at 500 °C, Solid State Ionics 129 (2000) 95–110.
[3] M. Gödickemeier, L.J. Gauckler, Engineering of solid oxide fuel cells with ceria-based electrolytes, Journal of the Electrochemical Society 145 (2) (1998) 414–421.
[4] J.V. Herle, T. Horita, T. Kawada, N. Sakai, H. Yokokawa, M. Dokiya, Fabrication and sintering of fine yttria-doped ceria powder, Journal of the American Ceramic Society 80 (1997) 933–940.
[5] H. Yahiro, K. Eguchi, H. Arai, High temperature fuel-cell with ceria-yttria solid electrolyte, Journal of the Electrochemical Society 135 (1988) 2077–2080.
[6] M. Yashima, T. Takizawa, Atomic displacement parameters of ceria doped with rare-earth oxide $Ce_{0.8}R_{0.2}O_{1.9}$ (R = La, Nd, Sm, Gd, Y, and Yb) and correlation with oxide-ion conductivity, Journal of Physical Chemistry C 114 (2010) 2385–2392.
[7] Y.P. Fu, S.H. Chen, J.J. Huang, Preparation and characterization of $Ce_{0.8}M_{0.2}O_{2-\delta}$ (M = Y, Gd, Sm, Nd, La) solid electrolyte materials for solid oxide fuel cells, International Journal of Hydrogen Energy 35 (2010) 745–752.
[8] V.P. Kumar, Y.S. Reddy, P. Kistaiah, G. Prasad, C.V. Reddy, Thermal and electrical properties of rare-earth co-doped ceria ceramics, Materials Chemistry and Physics 112 (2008) 711–718.
[9] I. Kosacki, H.U. Anderson, Y. Mizutani, K. Ukai, Nonstoichiometry and electrical transport in Sc-doped zirconia, Solid State Ionics 152–153 (2002) 431–438.
[10] V. Grover, A. Banerji, P. Sengupta, A.K. Tyagi, Raman XRD and microscopic investigations on CeO_2–Lu_2O_3 and CeO_2–Sc_2O_3 systems: a sub-solidus phase evolution study, Journal of Solid State Chemistry 181 (2008) 1930–1935.
[11] A. Moure, J. Tartaj, C. Moure, Synthesis sintering and electrical properties of yttria–calcia-doped ceria, Journal of the European Ceramic Society 29 (2009) 2559–2565.

[12] A. Moure, T. Hungria, A. Castro, J. Galy, O. Peña, J. Tartaj, C. Moure, Mechanosynthesis of the orthorhombic perovskites $ErMn_{1-x}Ni_xO_3$ ($x = 0$, 0.1). Processing and characterization of nanostructured ceramics, Chemistry of Materials 22 (2010) 2908–2915.

[13] A. Moure, J. Tartaj, C. Moure, Single-phase ceramics with $La_{1-x}Sr_xGa_{1-y}Mg_yO_{3-\delta}$ composition from precursors obtained by mechanosynthesis, Journal of Power Sources 196 (2011) 10543–10549.

[14] J.E. Bauerle, Study of solid electrolyte polarization by a complex admittance method, Journal of Physics and Chemistry of Solids 30 (1969) 2657–2670.

[15] A. Moure, A. Castro, J. Tartaj, C. Moure, Mechanosynthesis of perovskite $LaGaO_3$ and its effect on the sintering of ceramics, Ceramics International 35 (2009) 2659–2665.

[16] G.C.C. Costa, R. Muccillom, Synthesis of scandia-stabilized zirconia nanoparticles by the polyacrylamide technique, Solid State Ionics 179 (2008) 1219–1222.

[17] P. Duran, C. Moure, J.R. Jurado, Sintering and microstructural development of ceria–gadolinia dispersed powders, Journal of Materials Science 29 (1994) 1940–1948.

[18] X. Gang, Y.W. Zhang, C.S. Liao, C.H. Yan, Grain size-dependent electrical conductivity in scandia-stabilized zirconia prepared by a mild urea-based hydrothermal method, Solid State Ionics 166 (2004) 391–396.

[19] S. Omar, E.D. Wachsman, J.L. Jones, J.C. Nino, Crystal structure–ionic conductivity relationships in doped ceria systems, Journal of the American Ceramic Society 92 (11) (2009) 2674–2681.

[20] F. Ye, T. Mori, D.R. Ou, M. Takahashi, J. Zou, J. Drennan, Ionic conductivities and microstructures of ytterbium-doped ceria, Journal of the Electrochemical Society 154 (2007) B180–B185.

[21] T. Mori, J. Drennan, J.H. Lee, J.G. Li, T. Ikegami, Oxide ionic conductivity and microstructures of Sm- or La-doped CeO_2-based systems, Solid State Ionics 154–155 (2002) 461–466.